European Journal of Pharmaceutical Sciences 212 (2025) 107211

Contents lists available at ScienceDirect

European Journal of Pharmaceutical Sciences

journal homepage: www.elsevier.com/locate/ejps

Metastasis and angiogenesis: preclinical PET study on hepatocellular carcinoma (He/De) tumor models

Alexandra Barkóczi [a,b,1], Zita Képes [c,d,1,*], Judit P. Szabó [c], Renáta Adél Dienes [c,d], Péter Kálmán Károlyi [d,e,f], Tamás Papp [e,f], Ibolya Kálmán-Szabó [c,d], Tamás Sass [g], Gábor Opposits [c], István Kertész [c], István Hajdu [c], György Trencsényi [c,d], Ádám Deák [a,b]

[a] Department of Operative Techniques and Surgical Research, Faculty of Medicine, University of Debrecen, Moricz Zsigmond St. 22 H-4032 Debrecen, Hungary
[b] Doctoral School of Clinical Medicine, University of Debrecen, Nagyerdei St. 98 H-4032 Debrecen, Hungary
[c] Division of Nuclear Medicine and Translational Imaging, Department of Medical Imaging, Faculty of Medicine, University of Debrecen, Nagyerdei St. 98 H-4032 Debrecen, Hungary
[d] Gyula Petrányi Doctoral School of Clinical Immunology and Allergology, Faculty of Medicine, University of Debrecen, Nagyerdei St. 98 H-4032 Debrecen, Hungary
[e] Division of Radiology and Imaging Science, Department of Medical Imaging, Faculty of Medicine, University of Debrecen, Nagyerdei St. 98 H-4032 Debrecen, Hungary
[f] Doctoral School of Neuroscience, Faculty of Medicine, University of Debrecen, Nagyerdei St. 98 H-4032 Debrecen, Hungary
[g] Department of Surgery, Faculty of Medicine, University of Debrecen, Nagyerdei St. 98 H-4032 Debrecen, Hungary

ARTICLE INFO

Keywords:
angiogenesis
[^{68}Ga]Ga-NOTA-c(NGR)
[^{68}Ga]Ga-NODAGA-[c(RGD)]$_2$
hepatocellular carcinoma (He/De)
metastasis
positron emission tomography (PET)

ABSTRACT

The use of animal models to study tumorigenesis and metastatic spread seems crucial to discover novel diagnostic and therapeutic targets that inhibit tumor development and progression. In this study a preclinical metastasis model of hepatocellular carcinoma (He/De) was established to explore metastases formation and related angiogenic processes using positron emission tomography (PET) and angiogenesis specific radiopharmaceuticals. Approximately 8 ± 1 days after the subrenal capsule assay-based generation of the primary, secondary and tertiary transplanted metastatic He/De tumors in Fischer-344 rats, we used [^{18}F]FDG, [^{68}Ga]Ga-NOTA-c(NGR) and [^{68}Ga]Ga-NODAGA-[c(RGD)]$_2$ for the *in vivo* PET imaging of tumor development and angiogenesis. [^{18}F]FDG displayed the highest level of radioactivity among all investigated tracers. This pattern was consistent across all neoplastic lesions in each of the three transplantations. Comparing the two ^{68}Ga-labelled probes, the NGR compound showed significantly higher accumulation in the subrenally growing primary/secondary/tertiary He/De tumors ($p \leq 0.05$) and related parathymic lymph node metastases (PTLNs, $p \leq 0.01$) that could indicate higher expression level for aminopeptidase N/CD13 than for RGD-binding $\alpha_v\beta_3$ integrin. Progressive increase in the [^{18}F]FDG, [^{68}Ga]Ga-NOTA-c(NGR) and [^{68}Ga]Ga-NODAGA-[c(RGD)]$_2$ uptakes of both the subrenally growing He/De tumors and the PTLNs during the serial transplantations may imply increasing aggressivity. Overall, the currently developed experimental system provides a feasible platform for further investigation of metastatic spread.

1. Introduction

Even though remarkable advancements have been made in cancer research over the past decades (Ando et al., 2021; Biemar and Foti, 2013) metastases formation and disease dissemination still constitute the major cause of tumor-related mortality (Guan, 2015; Parker et al.,

Abbreviations: APN/CD13, aminopeptidase N; DMEM, Dulbecco's Modified Eagle Medium; FBS, foetal bovine serum; ^{68}Ga, Gallium-68; He/De, hepatocellular carcinoma; IVC, individually ventilated cages; ML-EM, Maximum-Likelihood Expectation-Maximization; My1/De, acute myelomonoblastic leukemia; My2/De, acute myelomonoblastic leukemia ; Ne/De, mesoblastic nephroma; NGR, asparagine-glycine-arginine; PET, positron emission tomography; PTLN, thoracic parathymic lymph node; RGD, arginine-glycine-asparagine; SD, standard deviation; SRCA, Subrenal Capsule Assay; SUV, standardized uptake value; T/M, tumor-to-muscle ratio; VOI, volume of interest.

* Corresponding author at: Division of Nuclear Medicine and Translational Imaging, Department of Medical Imaging, Faculty of Medicine, University of Debrecen, Nagyerdei St. 98 H-4032 Debrecen, Hajdú Bihar County, Hungary.
E-mail address: kepes.zita@med.unideb.hu (Z. Képes).
[1] These authors contributed equally to this work.

https://doi.org/10.1016/j.ejps.2025.107211
Received 6 January 2025; Received in revised form 17 July 2025; Accepted 20 July 2025
Available online 20 July 2025

2022; Seyfried and Huysentruyt, 2013). Therefore, uncovering the pathophysiological underpinnings of metastatic spread seems pivotal to discover diagnostic target candidates for early lesion identification and therapeutic planning.

Nowadays, the use of preclinical tumor models represents a cornerstone of modern cancer research in the field of biological sciences (Sajjad et al., 2021). As these experimental systems recapitulate the complexity of tumorigenesis and metastasis formation (Sharma et al., 2023) they serve as unique tools to address the multifaceted nature of cancer biology at preclinical level (Arató et al., 2024; Liu et al., 2023; Wakefield et al., 2023). Besides allowing for the investigation of associated processes in real time and *in vivo* (Cunha et al., 2014; Sajjad et al., 2021) experiments with cancer models may lead to the exploration of novel diagnostic and therapeutic biomarkers. For example, graphene nanomesh-based platforms have demonstrated highly efficient photothermal therapy in U87MG human glioblastoma models, highlighting the utility of such systems in evaluating advanced nanotherapeutics (Akhavan and Ghaderi, 2013). Likewise, multifunctional gold@-graphene oxide (Au@GO) core-shell nanoplatforms have demonstrated enhanced miRNA delivery (miRNA-101) *in vitro*, and when combined with NIR-mediated (near infrared) thermal therapy achieved over 80 % reduction in breast cancer cell viability (Assali et al., 2018). Similar nanoplatforms co-loaded with doxorubicin induced tumor suppression in 4T1 breast tumor-bearing mice under NIR irradiation (NRGO-GNS@DOX), indicating their potential in targeted and efficient therapeutic strategies (Wang et al., 2016). Therefore, beyond their role in drug development, preclinical model systems also provide cost-effective platforms for testing novel therapeutic candidates (Mukherjee et al., 2022).

Based on literature data, low expenses, easy handling and short lifetime make rodents the most widely used laboratory animals for the establishment of tumor models (Eur. Comm. 2019, 2019; Glenny et al., 2021). Because of their small size, more sustainable maintenance and favourable genetic background, mice are often preferable to rats (Bryda, 2013). Nevertheless, rats perform better in mimicking human genetics, anatomy and physiology (Cyagen Knockout Catalog Models, 2020) that should also be considered upon selecting the best fitting rodent model. Given their larger body sizes, rats are favoured in investigations requiring invasive techniques (Bryda, 2013; Kwitek-Black and Jacob, 2001) such as surgical interventions or tissue removal. For instance, the *in vivo* biodistribution and tumor-targeting potential of ^{198,199}Au-labelled graphene oxide nanostructures ((198,199)Au@AF-GO) has been successfully evaluated in rat models of fibrosarcoma with single-photon emission computed tomography (SPECT) technique, highlighting their suitability for advanced nuclear imaging applications (Fazaeli et al., 2014). A wide variety of rodent metastatic models are available to assess the multi-step process of metastatic propagation. These models can be used to assess key stages including tumor cell dissemination, invasion, extra, - or intravasation, and seeding (Giacobbe and Abate-Shen 2021; Hebert et al., 2023). Based on literature data, metastatic models derived from cell lines revealed the most about metastasis development, tumor cell migration, as well as the genetic determinants of related processes (Fidler 1970; Hart and Fidler, 1980; Kang et al., 2003; Minn et al., 2005).

Positron emission tomography (PET) is one of the most suitable imaging modalities to *in vivo* investigate the pathophysiological background of cancer initiation as well as dissemination in preclinical tumor models (Cunha et al., 2014; Miranda et al., 2021). Using radiopharmaceuticals, PET ensures to non-invasively track tumor-associated biochemical and functional processes even repeatedly at molecular level (Phelps, 2000a; Phelps 2000b). Prior *in vivo* PET studies with My1/De (Arató et al., 2024) and My2/De (Trencsenyi et al., 2014a) myelomonoblastic leukemia rat models for example provided valuable insights into tumor propagation and metastatic patterns. In these works My1/De and My2/De leukemic cells placed under the left renal capsule were shown to disseminate to various abdominal organs and to the mesenterial and thoracic parathymic lymph nodes (PTLNs), supporting the utility of these models for evaluating metastatic spread *in vivo*. As one of the major contributors of tumor development and maintenance, angiogenesis could also be effectively studied with preclinical systems of tumor metastases (Kuczynski et al., 2016; Nolan et al., 2007; Wong et al., 2015). Several PET vectors targeting angiogenic biomarkers like integrin alphaVbeta3 (integrin $a_v\beta_3$, *e.g.* [^{68}Ga]Ga-NODAGA-RGD (Shao et al., 2014a) or [^{68}Ga]Ga-NODAGA-[c(RGD)]$_2$ (Máté et al., 2015); NODAGA-RGD: cyclo[-Arg-Gly-Asp-D-Tyr-Lys (NODAGA)-], NODAGA-RGD dimer: NODAGA-Glu(cyclo[-Arg--Gly-Asp-D-Tyr-Lys-]$_2$) or aminopeptidase N (APN/CD13, *e.g.* [^{68}Ga]Ga-NOTA-cNGR; NOTA-cNGR: cyclo[-Lys(NOTA-Bn-NCS)-Asn-Gly-Arg--Glu-]-CONH$_2$) (Bieker et al., 2009; Zhu et al., 2020; Zucali et al., 2013) are applicable to monitor tumor-related neoangiogenic changes *in vivo*. With established animal models of mesoblastic nephroma (Ne/De) tumors, our research team published for the first time that target-selective radiolabelled probes serve as valuable means to monitor alterations of cell surface biomarkers in relation to angiogenesis during tumor development (Szabo et al., 2022). Focusing on the microPET imaging of subrenally growing primary Ne/De tumors and serially transplanted PTLN metastases with NGR/RGD-based radiotracers, in this work Szabo et al. observed increasing tumor tracer accumulations during the dissemination process that may imply enhanced angiogenic activity and malignancy. In addition, in former papers we published that similarly to Ne/De tumors, the subrenal transplantation of hepatocellular carcinoma cells (He/De), though with slower dynamics, led to metastases development in the PTLN (Trencsenyi et al., 2014b).

While prior studies have expanded our understanding of the multistep process of tumorigenesis, numerous open questions still remain regarding metastatic spread and associated angiogenic changes. To address this gap, in this study we established a syngeneic metastatic rat model of hepatocellular carcinoma, and applied complexes of NGR and RGD compounds labelled with ^{68}Ga ([^{68}Ga]Ga-NODAGA-[c(RGD)]$_2$/[^{68}Ga]Ga-NOTA-c(NGR)) to investigate tumor-related angiogenic processes with PET technique.

2. Materials and methods

2.1. Preparation of the study animals

Thirty male adult (16 weeks old, 250±20 g) Fischer-344 rats were used in this study. Principles of the Ethics Committee for Animal Experimentation of the United Kingdom were followed, and the local Ethics Committee for Animal Experimentation approved the experiment (University of Debrecen, approval number: 28/2023/DEMÁB). The animals were kept in individually ventilated cages (IVC) in a temperature (26 °C ± 2 °C) and humidity (51±10 %)-controlled room with a 12-hour light/12-hour dark schedule. Tap water and semi-synthetic rodent food were provided *ad libitum* (Animalab, Budapest, Hungary) for all study rats.

2.2. Preparation of He/De tumor cells and cell culturing

Chemically induced He/De tumor model was established by the intraperitoneal injection of 125 µg n-nitrosodimethylamine (Merck, Darmstadt, Germany) into Fischer-344 rats (Trencsenyi et al., 2014b). After 6 months the He/De tumors were extracted, and corresponding cell line was established. The cells were cultivated under standard conditions (37 °C, 95 % relative humidity, 5 % CO_2/95 % air) in Dulbecco's Modified Eagle Medium (DMEM, Merck Ltd., Budapest, Hungary) supplemented with 10 % foetal bovine serum (FBS), 100 unit/mL penicillin and 100 mg/mL streptomycin. Cell culture passage was performed 3 times weekly. The cell lines were tested for mycoplasma contamination and found to be negative.

2.3. Serial tumor transplantation

Using 1.5 % Forane, (AbbVie, Budapest, Hungary; OGYI-T-1414/01),

0.4 L/min O_2 (Linde Healthcare, Budapest, Hungary; OGYI-T-20,607), and 1.2 L/min N_2O (Linde Healthcare; OGYI-T-21,090) all animals were anaesthetized before the experiments in a dedicated small animal anaesthesia chamber. Tumor cell transplantation was accomplished using Subrenal Capsule Assay (SRCA) technique based on a method described earlier by Trencsényi et al. (Trencsenyi et al., 2009). Briefly, after shaving off the fur of the left lumbar region, the peritoneal lining, and all tissues within were carefully intersected to access the retroperitoneal space. Once extracted, 1×10^6 He/De cells dissolved in 10 μL physiological saline solution (0.9 % NaCl solution) were inoculated on a Gelaspon^R gauze (Germed, Rudolstadt, Germany) under the left renal capsule of Fischer-344 rats *(primary transplantation)*. Approximately 8 ± 1 days post tumor cell inoculation, the metastatic thoracic PTLNs of the primary He/De tumors were further subrenally transplanted into healthy rats using the same SRCA method *(serial transplantations)*. This process (subrenal implementation of the metastatic PTLNs) was conducted overall twice. After the interventions, surgical suturing was performed that was followed by the administration of non-steroid anti-inflammatory analgesic (Nurofen syrup 10 mg/kg) in drinking water *ad libitum* (Dezso et al., 1990).

2.4. Preparation of the radiopharmaceuticals

The glucose analogue [^{18}F]FDG was synthesised and labelled with the positron decaying isotope ^{18}F according to the GMP-certified pharmaceutical manufacturing method of the Department of Nuclear Medicine (Faculty of Medical Imaging, University of Debrecen, Debrecen, Hungary). [^{68}Ga]Ga-NOTA-c(NGR) and [^{68}Ga]Ga-NODAGA-[c(RGD)]$_2$ targeting APN/CD13 and $\alpha_v\beta_3$; respectively were synthesized based on the methods described earlier by our research team (Kis et al., 2020; Máté et al., 2015).

2.5. Rat PET imaging with [^{68}Ga]Ga-NOTA-c(NGR)/[^{68}Ga]Ga-NODAGA-[c(RGD)]$_2$/[^{18}F]FDG

PET imaging was accomplished applying the MiniPET-II scanner of the preclinical laboratory of the Division of Nuclear Medicine and Translational Imaging (Faculty of Medicine, Department of Medical Imaging, University of Debrecen, Debrecen, Hungary). The subrenally developing tumors were allowed to grow for 8 ± 1 days to reach a tumor volume suitable for PET scanning. Prior to imaging with the angiogenesis specific compounds, [^{18}F]FDG was applied to verify the presence of the tumors. The intravenous injection of approx. 7 MBq of [^{18}F]FDG, [^{68}Ga]Ga-NOTA-c(NGR) and [^{68}Ga]Ga-NODAGA-[c(RGD)]$_2$ was completed in 0.15 mL physiological saline solution as a bolus (specific activities: 5.47±0.36 GBq/μmol, 9.82±1.08 GBq/μmol and 40 GBq/μmol for [^{68}Ga]Ga-NOTA-c(NGR), [^{68}Ga]Ga-NODAGA-[c(RGD)]$_2$ and [^{18}F]FDG; respectively, injected volume: 150 μL). Thereafter, 20-minute static PET acquisition was performed on the thoracic and abdominal regions (kidneys) of all experimental rats 50 and 90 min post administration of [^{18}F]FDG and the 68-Gallium labelled tracers; respectively. Isoflurane-induced anaesthesia was maintained during the whole imaging period.

2.6. PET data processing and image analyses

Followed by data post-processing with 2D ML-EM iterative image reconstruction, PET images were stored in a MultiModal Medical Imaging Software repository. Using quantitative BrainCad image analysis software, the tumors were covered with one volume of interest (VOI) on the coronal slices, and average/maximal radiopharmaceutical concentrations in the VOIs were expressed as standardized uptake values (SUVmean/SUVmax). Tumor-to-off target ratios were also defined from the radioactivity concentration of the tumor and the reference background skeletal muscle tissue from the region of the scapula (T/M/tumor-to-muscle ratio). In addition, uptake rates were compared between the three investigated radiopharmaceuticals ([^{68}Ga]Ga-NOTA-c(NGR)/[^{68}Ga]Ga-NODAGA-[c(RGD)]$_2$/[^{18}F]FDG).

2.7. Statistical analyses

Quantitative data are presented as mean±SD of at least three independent experiments. The significance was calculated by Student's t test (two-tailed), two-way ANOVA, and Mann-Whitney rank-sum tests. A P value ≤ 0.05 was considered as significant. For the accomplishment of all data analyses, we used MedCalc 18.5 (MedCalc Software, Mariakerke, Belgium) commercial software package.

3. Results

3.1. Visual analyses

To assess the differences between the tumor uptake of the three radiotracers *in vivo* PET imaging was conducted in He/De tumor-bearing rats. Representative decay-corrected PET scans on the first, second and third SRCA transplantations are shown in Fig. 1, 2 and 3; respectively. Visually, the subrenally growing He/De tumors (both the primary He/De and the transplanted metastatic PTLNs) absorbed all three investigated radiotracers ([^{68}Ga]Ga-NOTA-c(NGR)/[^{68}Ga]Ga-NODAGA-[c(RGD)]$_2$ /[^{18}F]FDG), however, the most prominent tracer uptakes were detected in the tertiary tumors (Fig. 3**a**, second serial transplantation). Comparing the imaging performance of the radiolabelled glucose analogue and that of the ^{68}Ga-labelled derivatives, all He/De tumors could be best visualized with [^{18}F]FDG (Fig. 1**a**-3**a first column**). [^{68}Ga]Ga-NOTA-c(NGR) showed the second highest accumulation in the subrenally developing tumors (Fig. 1**a**-3**a second column**), and the least radioactivity was found for the RGD compound (Fig. 1**a**-3**a third column**). In a like manner, all [^{18}F]FDG, [^{68}Ga]Ga-NOTA-c(NGR) and [^{68}Ga]Ga-NODAGA-[c(RGD)]$_2$ performed well in identifying the PTLN metastases in the thorax, and the highest accumulations were also found in the tertiary metastases for all tracers (second serial transplantation, Fig. 3**b**). Similarly to the findings on the He/De tumors, we observed the greatest uptake of the PTLN metastases for [^{18}F]FDG, followed by [^{68}Ga]Ga-NOTA-c(NGR) and [^{68}Ga]Ga-NODAGA-[c(RGD)]$_2$ in case of all transplantations (Fig. 1**b**-3**b**). Overall, the metastatic PTLNs in the thorax showed less intense radioactivity for all compounds in comparison with that of the He/De tumors under the kidney capsule.

3.2. Quantitative PET analyses

8 ± 1 days after the subrenal transplantation of He/De cells, the SUVmean and SUVmax values of the primary tumors were the highest for [^{18}F]FDG (Table 1), and this reached statistically notable difference from the uptake of both the NGR *($p \leq 0.01$)* and the RGD probe *($p \leq 0.01$)* (Fig. 4 **Panel a**). The second highest radioactivity for the primary He/De tumors was found with the administration of [^{68}Ga]Ga-NOTA-c(NGR), followed by [^{68}Ga]Ga-NODAGA-[c(RGD)]$_2$ (Fig. 4 **Panel a**, Table 1). Though only at $p \leq 0.05$, the radioactivity of the two angiogenic vectors also differed statistically significantly.

Consistent with the visual observations, similar uptake tendency was experienced in case of the secondary and the tertiary He/De tumors with the highest radioactivity detected for the [^{18}F]FDG scans and least for the radiolabelled RGD images (Fig. 5,6 **Panel a**, Table 1). Accordingly, the secondary He/De tumors showed more prominent radioactivity with [^{18}F]FDG in comparison with both [^{68}Ga]Ga-NOTA-c(NGR) and [^{68}Ga]Ga-NODAGA-[c(RGD)]$_2$ (Fig. 5 **Panel a**, Table 1). These differences were statistically significant at $p \leq 0.05$ and $p \leq 0.01$ for the NGR and the RGD derivatives; respectively. In addition, similarly to the findings on the primary He/De tumors, [^{68}Ga]Ga-NOTA-c(NGR) accumulated to a greater extent in the transplanted primary PTLN metastasis (secondary He/De tumor, Table 1) compared to the RGD vector *($p \leq 0.05$)*.

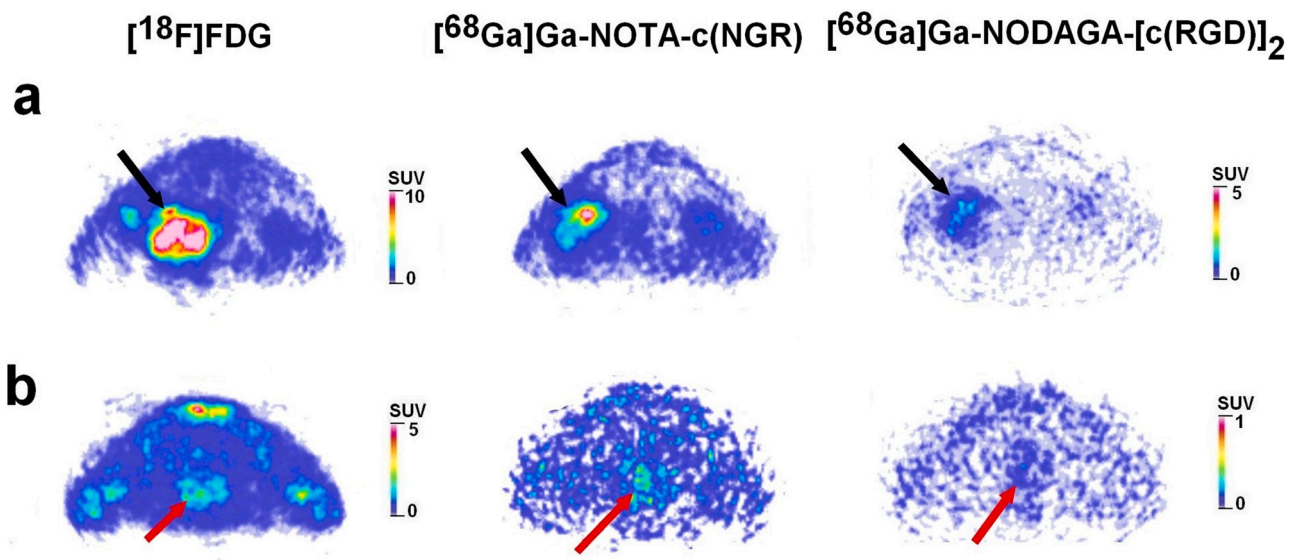

Fig. 1. A series of static micro-PET images 8 ± 1 days after the subrenal transplantation of He/De tumors cells. **a)** Primary He/De tumors under the left renal capsule and **b)** (primary) metastatic thoracic parathymic lymph nodes visualized 50 min post [^{18}F]FDG administration, and 90 min post [^{68}Ga]Ga-NOTA-c(NGR) and [^{68}Ga]Ga-NODAGA-[c(RGD)]$_2$ injection. Primary tumors and the metastases are delineated with black and red arrows; respectively. *He/De: hepatocellular carcinoma; PET: positron emission tomography.*

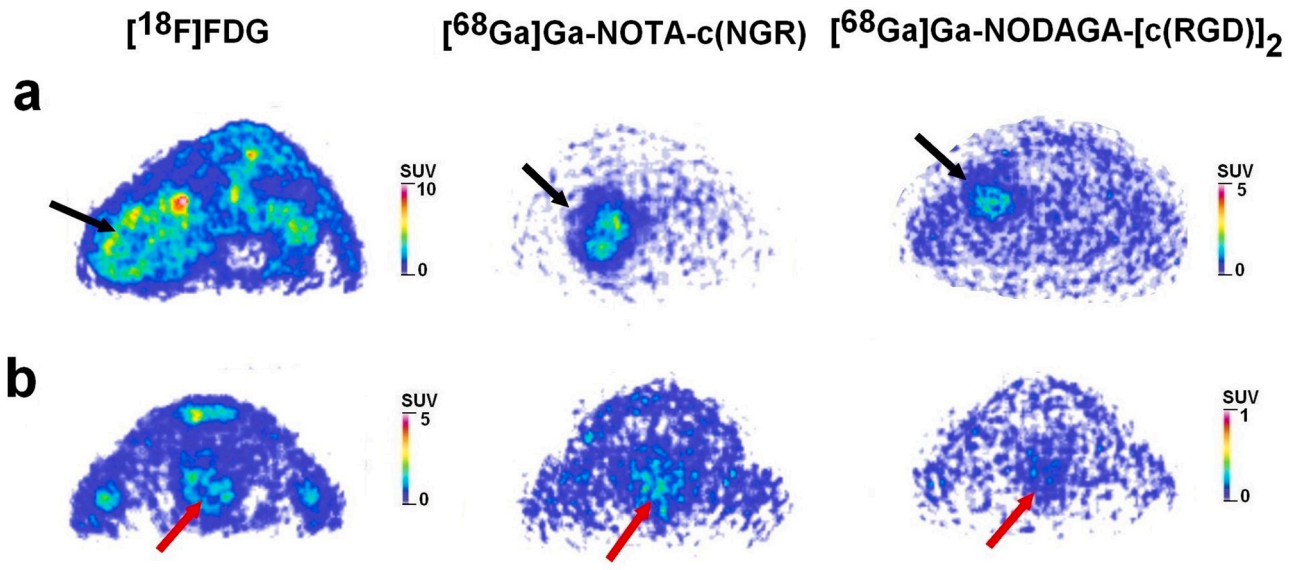

Fig. 2. Static micro-PET imaging results 8 ± 1 days after the subrenal transplantation of the metastatic thoracic parathymic lymph node derived from the primary He/De tumor **a)** Subrenally growing secondary He/De tumors and **b)** (secondary) metastatic thoracic parathymic lymph nodes. PET imaging was performed using [^{18}F]FDG (50 min), and ^{68}Ga-labelled peptide compounds (90 min). The secondary He/De tumors and the metastases are annotated with black and red arrows; respectively. *He/De: hepatocellular carcinoma; PET: positron emission tomography.*

Comparable to the uptakes of both the primary and the secondary He/De tumors, approximately 8 days post SRCA transplantation of the secondary metastatic PTLN, the highest tracer concentration in the tertiary He/De tumor was also found with [^{18}F]FDG followed by [^{68}Ga]Ga-NOTA-c(NGR) and [^{68}Ga]Ga-NODAGA-[c(RGD)]$_2$ (Table 1, Fig. 6 **Panel a**). The distinctions between the accumulation of [^{18}F]FDG and that of the ^{68}Ga-labelled NGR/RGD molecules were significant at $p \leq 0.01$ and these were in line with the observations on the primary He/De tumors. The quantitative SUV data of the He/De tumors are presented in Table 1.

As shown in Fig. 1**b**-3**b**, the accumulation kinetics of the PTLN metastases was comparable to that of the subrenally growing tumors, though, much lower radioactivity concentrations were registered (seen in Fig. 4**b**-6**b**). Similarly to the He/De tumors (all the primary/secondary/tertiary), the SUV values of metastatic PTLNs were the highest with the radiolabelled glucose derivative (SUVmean: 2.94±0.87; SUVmax: 8.64±1.36 Fig. 4**b**, SUVmean: 3.14±0.64; SUVmax: 9.07±1.07 Fig. 5**b**, and SUVmean: 4.59±1.21; SUVmax: 12.63±2.17 Fig. 6**b** for the 1st, 2nd and 3rd transplantations; respectively, Table 2) that reached statistical significance from the uptake figures of the angiogenic tracers *($p \leq 0.01$)*.

Comparing the accumulation of the ^{68}Ga-labelled peptide probes in the PTLN metastases - in accordance with the He/De tumors - higher retention was found for the [^{68}Ga]Ga-NOTA-c(NGR) PET scans in case of all three transplantations than for the RGD images, and this difference tended to be statistically significant at *($p \leq 0.01$)*, apart from the difference between the SUVmax data of the 1st SRCA operation for the

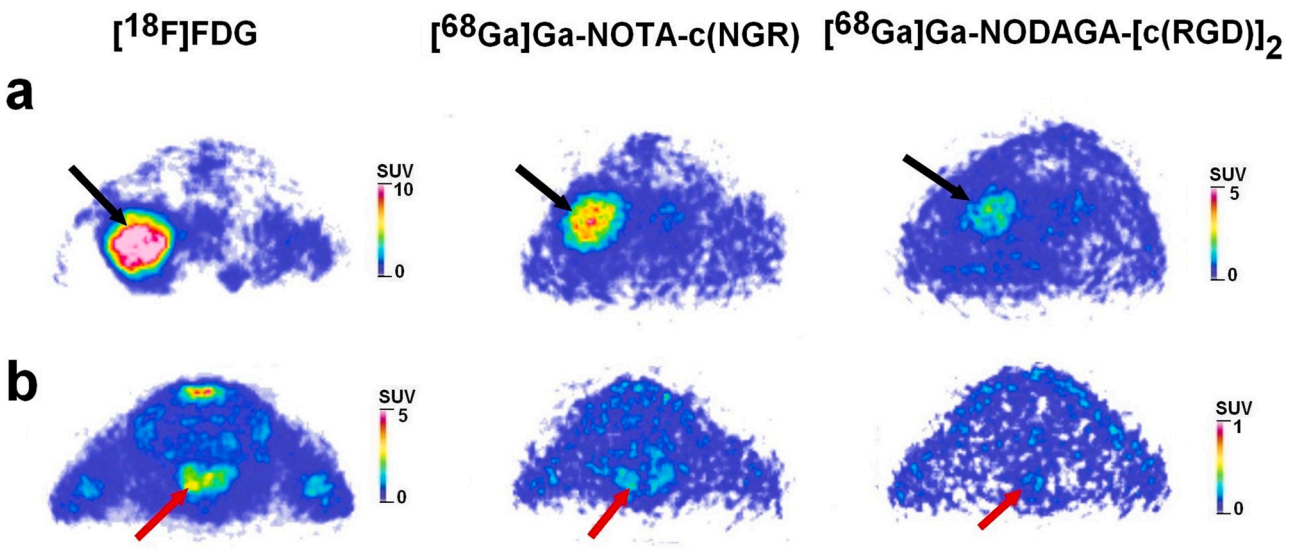

Fig. 3. Static PET images acquired 8 ± 1 days after the subrenal transplantation of the metastatic thoracic parathymic lymph node originating from the secondary He/De tumor. **a)** Tertiary He/De tumors under the left kidney capsule and **b)** metastatic thoracic parathymic lymph nodes (tertiary). PET images were captured 50 min after the injection of [^{18}F]FDG, and 90 min after the injection of [^{68}Ga]Ga-NOTA-c(NGR) and [^{68}Ga]Ga-NODAGA-[c(RGD)]$_2$. Black arrows point to the secondary He/De tumors, red arrows indicate the metastatic lymph nodes. *He/De: hepatocellular carcinoma; PET: positron emission tomography.*

Table 1
Quantitative SUV analyses of [^{18}F]FDG, [^{68}Ga]Ga-NOTA-c(NGR) and [^{68}Ga]Ga-NODAGA-[c(RGD)]$_2$ in subrenally growing He/De tumors 8 ± 1 days after the SRCA-based transplantation of He/De tumor cells (1st transplantation), the primary metastatic PTLN (2nd transplantation) and the secondary metastatic PTLN (3rd transplantation), and 50 ([^{18}F]FDG) and 90 (^{68}Ga-labelled tracers) minutes post radiotracer injection. The uptake values are presented as mean±SD.

	Subrenal tumors	[^{18}F]FDG	[^{68}Ga]Ga-NOTA-c(NGR)	[^{68}Ga]Ga-NODAGA-[c(RGD)]$_2$
1st transplantation	SUVmean	6.89±1.84	3.69±0.64	1.34±0.61
	T/M SUVmean	6.13±0.80	14.87±2.46	8.85±2.42
	SUVmax	12.24±2.63	8.64±0.94	4.67±1.34
	T/M SUVmax	8.35±1.63	20.82±2.53	15.74±1.86
2nd transplantation	SUVmean	7.36±1.67	3.78±0.47	2.21±0.61
	T/M SUVmean	7.61±1.42	17.62±3.81	12.07±3.08
	SUVmax	14.25±2.09	8.99±1.27	5.09±0.97
	T/M SUVmax	9.84±2.06	26.51±2.59	18.95±2.97
3rd transplantation	SUVmean	8.26±1.20	5.09±1.22	2.84±0.51
	T/M SUVmean	8.69±1.58	22.41±3.47	16.21±2.47
	SUVmax	16.74±2.67	10.75±2.31	6.31±1.08
	T/M SUVmax	11.25±2.34	28.36±4.12	21.64±2.61

^{68}Ga: Gallium-68; He/De: hepatocellular carcinoma; PTLN: parathymic lymph node; SD: standard deviation; SRCA: subrenal capsule assay; SUV: standardized uptake value; T/M: tumor-to-muscle ratio.

NGR-RGD probe that reached considerable difference only at $p \leq 0.05$ (as presented in Table 2). Furthermore, similarly to the subrenally growing tumors all tracer accumulations of the metastatic PTLNs showed a continuous increase during the serial transplantations (Table 2).

To evaluate which tracer provides the best-contrasted PET images, T/M ratios were calculated from the SUV values of the He/De tumors/metastatic PTLNs and that of the background muscle tissue (shown in Table 1 and Table 2). In case of the first SRCA transplantation, lower [^{68}Ga]Ga-NOTA-c(NGR) and [^{68}Ga]Ga-NODAGA-[c(RGD)]$_2$ uptakes of the non-target organs - compared to [^{18}F]FDG - along with notable tracer accumulation in the primary He/De tumors led to significantly higher tumor-to-background ratios for the NGR/RGD compounds ($p \leq 0.01$ for [^{68}Ga]Ga-NOTA-c(NGR) and $p \leq 0.05$ for [^{68}Ga]Ga-NODAGA-[c(RGD)]$_2$) than for the glucose analogue (Fig. 4 **Panel c,** Table 1). Regarding the primary metastatic PTLN, however, PET images with higher contrast were obtained with [^{18}F]FDG and [^{68}Ga]Ga-NOTA-c(NGR) (Fig. 4 **Panel d,** Table 2).

Similarly, more elevated T/M ratios were recorded for the two peptide-based probes than for [^{18}F]FDG in case of the secondary and the tertiary He/De tumors (Fig. 5 and 6 **Panel c**, Table 1), and the secondary/tertiary metastatic PTLN could also be better delineated form the background using [^{18}F]FDG and the NGR molecule (Fig. 5 and 6 **Panel d,** Table 2).

4. Discussion

Limited understanding of metastasis biology hampers the opening of novel diagnostic and therapeutic window for successful intervention. Therefore, to reveal yet uncovered aspects of this dissemination process, the role of *in vivo* model systems is emerging. Syngeneic rat model established by Trencsényi et al. (Trencsenyi et al., 2009) seems applicable for the evaluation of metastasis growth as well as corresponding angiogenic processes (Máté et al., 2015; Szabo et al., 2022; Trencsenyi et al., 2014a, 2014b). In correlation with the current experiences, they concluded that tumor cells placed under the left renal capsule of rats using SRCA propagate to the thoracic PTLNs via lymphatic channels. Also similar to their findings (Trencsenyi et al., 2009) the subrenally growing tumors as well as the thoracic metastases could be clearly detected using [^{18}F]FFDG. Although [^{18}F]FDG was highly taken up by the tumors, it lacks angiogenic specificity. Several studies have shown correlations between [^{18}F]FDG uptake and angiogenic markers

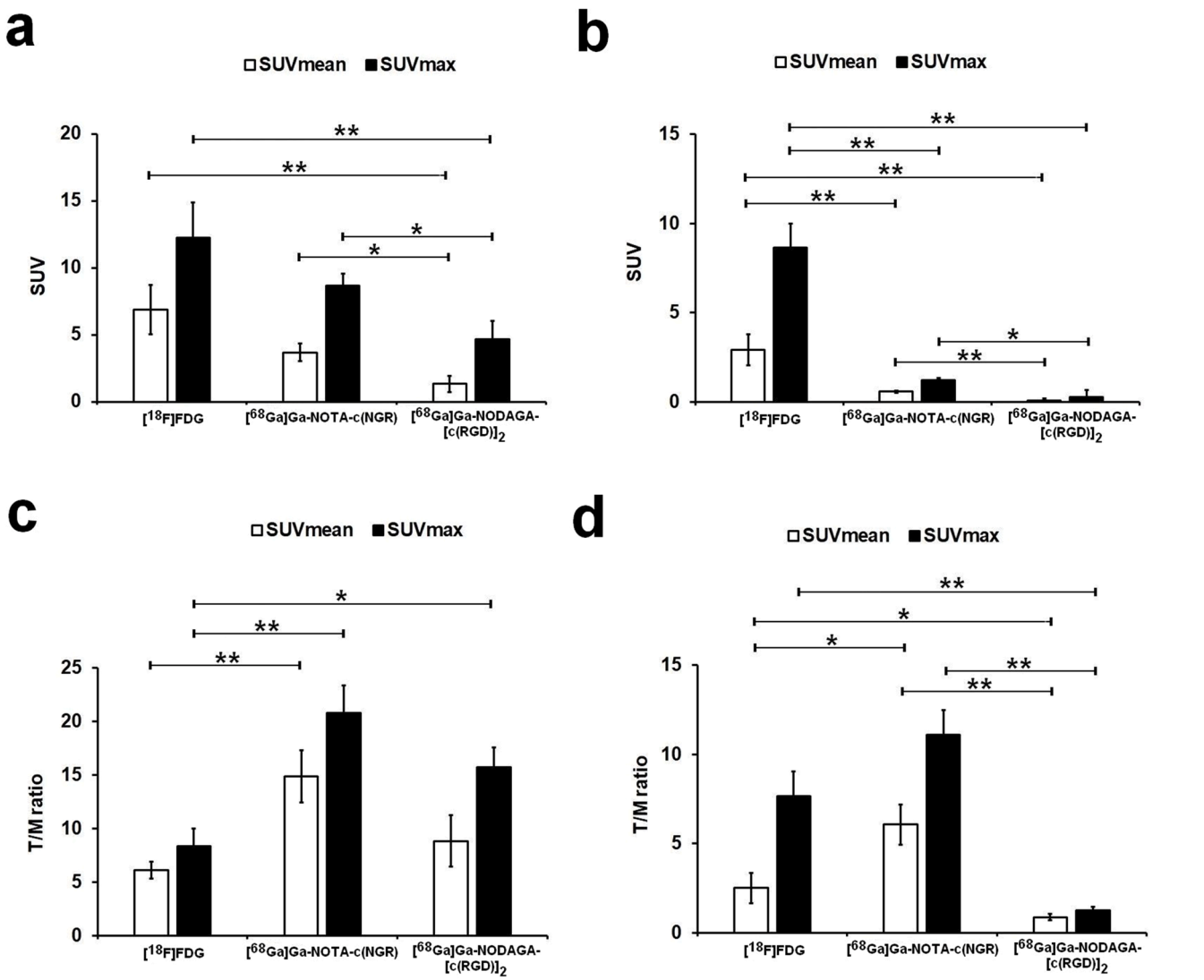

Fig. 4. Quantification of [^{18}F]FDG, [^{68}Ga]Ga-NOTA-c(NGR) and [^{68}Ga]Ga-NODAGA-[c(RGD)]$_2$ PET imaging in primary He/De tumors (**a** and **c**) and (primary) metastatic thoracic parathymic lymph nodes (**b** and **d**). SUV mean/max values and the T/M ratios were determined 50 min post [^{18}F]FDG and 90 min post NGR/RGD tracer injection. Statistical significance: (*) $p \leq 0.05$ and (**) $p \leq 0.01$. Data are presented as mean±SD; $n = 3$ rats/radiotracer. *SD: standard deviation; SUV: standardized uptake value; T/M: tumor-to-muscle ratio.*

including microvessel density (MVD) or GLUT1 transporters, however, the results are inconsistent and variable (Florea et al., 2021; Guo et al., 2006). For instance, Guo et al. (2006) observed no association between [^{18}F]FDG uptake and MVD in lung adenocarcinoma. Moreover, comparative studies with angiogenesis-specific tracers revealed distinct spatial distributions, suggesting that [^{18}F]FDG uptake may reflect overlapping but non-specific biological processes (Toriihara et al., 2019; Vatsa et al., 2019). Therefore, even though this radiolabelled glucose analogue properly represents tumor cell metabolism (Zhu et al., 2011), its lack of specificity (Jiang et al., 2014) presents challenges for its application in imaging tumor angiogenesis and associated receptor expression.

Substantial research has been made toward the development of radiotracers targeting angiogenic cell surface molecules that not only ensure to track the fate of tumor cells *in vivo* but may provide details on receptor biology and the mechanisms of metastasis progression. APN/CD13 (Kawamura et al., 2007; Murakami et al., 2005) and $\alpha_v\beta_3$ integrin (Cai and Chen, 2006; Weis and Cheresh, 2011) are abundantly overexpressed on most tumor types, hence radioactive ligands of these receptors allow for the specific imaging of pro-angiogenic molecules *in vivo* (Chen et al., 2013; Ma et al., 2013; Shao et al., 2014b). Several receptor-targeted peptide radiopharmaceuticals with APN-affine NGR (asparagine-glycyl-arginine; (Soudy et al., 2012)) and integrin selective RGD (arginine-glycine-asparagine; (Pasqualini et al., 2000)) sequences have been successfully synthesized and are widely used in the imaging of neoangiogenesis under preclinical conditions (Li et al., 2014; Ma et al., 2016; Shao et al., 2014a; Zhang et al., 2014). While [^{18}F]FDG is generally used to assess tumor (glucose) metabolism, NGR, - and RGD-based tracers, due to their specific binding affinity to receptors associated with angiogenesis, can selectively target neovasculature and related processes (Florea et al., 2021). This approach may be particularly advantageous in tumors with low [^{18}F]FDG uptake (*e.g.* well-differentiated hepatocellular carcinoma), or in those where angiogenesis plays a key role in disease progression (Gao et al., 2017). By offering potentially higher specificity and sensitivity, these peptides may allow for increased diagnostic accuracy and enhanced detection rates in certain tumor types compared to [^{18}F]FDG (Faintuch et al., 2014; Shao et al., 2014a). In addition, the advantages of RGD tracers over [^{18}F]FDG are becoming increasingly evident, particularly in the evaluation of head and neck tumors (Li et al., 2018; Zheng et al., 2019). Moreover, unlike [^{18}F]FDG, NGR/RGD peptides can be labelled with therapeutic radionuclides, enabling their use beyond imaging for

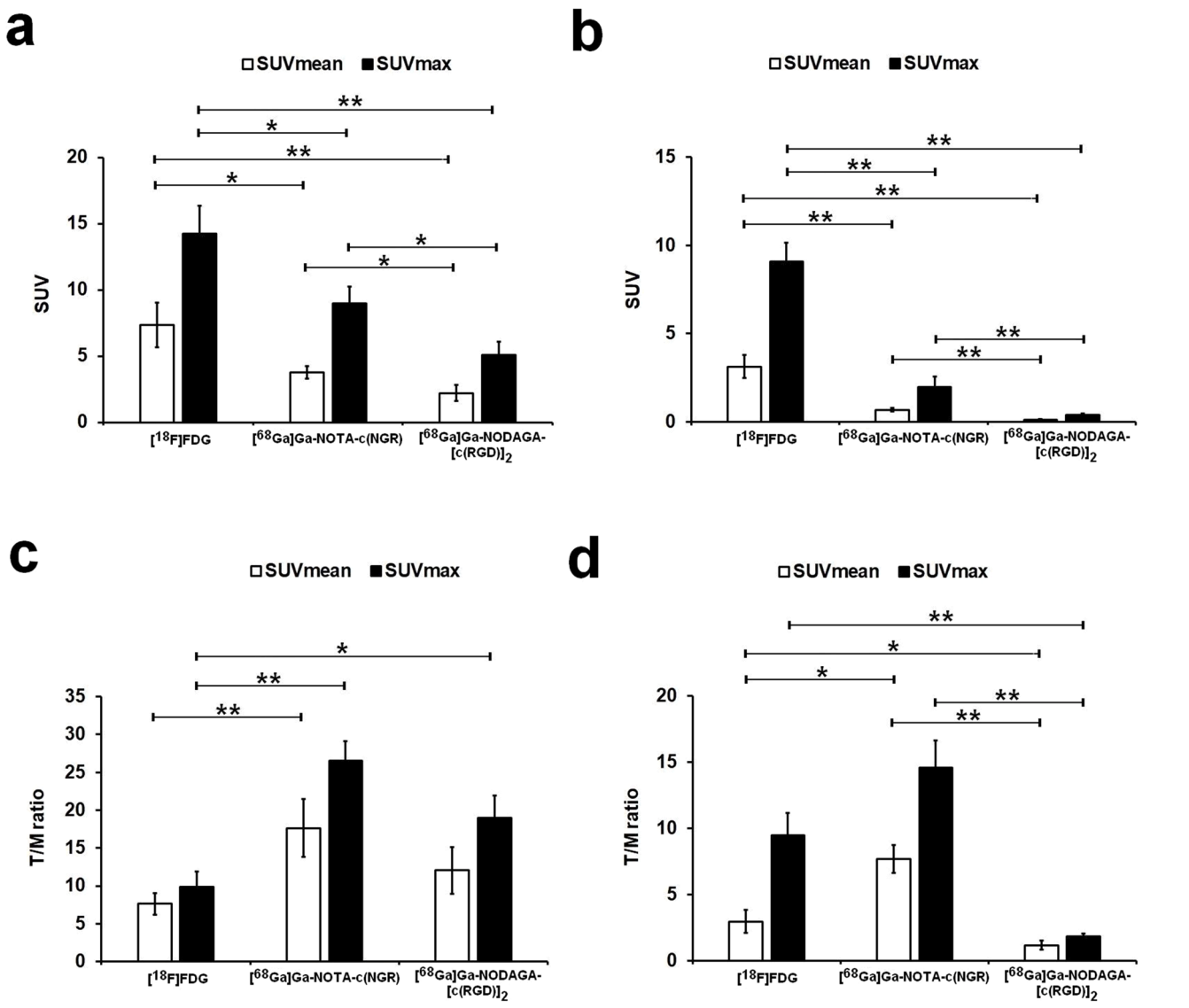

Fig. 5. Quantitative data on PET imaging with [^{18}F]FDG, [^{68}Ga]Ga-NOTA-c(NGR), and [^{68}Ga]Ga-NODAGA-[c(RGD)]$_2$ in secondary He/De tumors (**a** and **c**) and (secondary) thoracic parathymic lymph node metastases (**b** and **d**). SUV mean/max values (**a** and **b**) and tumor-to-muscle (T/M) ratios (**c** and **d**) were measured 50 and 90 min after [^{18}F]FDG and ^{68}Ga-labelled radiopharmaceutical injection; respectively. Asterisks indicate significance levels ($*p \leq 0.05$, $**p \leq 0.01$). Data are presented as mean±SD; $n = 3$ rats per radiotracer. *SD: standard deviation; SUV: standardized uptake value; T/M: tumor-to-muscle ratio.*

therapeutic purposes, and paving the way for theranostic strategies as well (Trencsényi et al., 2023).

In the present study all subrenally growing He/De tumors and the PTLN metastases were identifiable with the NGR/RGD tracers, that in accordance with literature findings, further strengthened the feasibility of these molecular probes in the detection of angiogenesis related to tumorigenesis and metastatic spread. Similarly, in prior studies using the renal capsule parathymic lymph node complex model (Rozsa et al., 2009; Trencsenyi et al., 2009) radiolabelled NGR/RGD molecules could also be successfully applied to track angiogenic processes and the presence of associated biomarkers (APN/CD13, $\alpha_v\beta_3$ integrin) (Máté et al., 2015; Szabo et al., 2022). Confirmed by Western blotting, Máté et al. (2015) for example verified the selective binding of [^{68}Ga]Ga-NOTA-c(NGR) to APN/CD13 using orthotopic Ne/De rat models. Likewise, in the PET study of Szabó et al. (2022), chemically induced Ne/De tumors and pertinent metastases could be monitored with radiolabelled NGR and RGD derivatives that also corresponded to the present findings. These NGR/RGD studies contrast with a recent preclinical PET imaging study using [^{18}F]cabozantinib, a multi-target tyrosine kinase inhibitor (TKI), that demonstrated poor tumor uptake and high non-specific binding (Lien et al., 2021), underscoring the superior tumor specificity of the receptor-selective NGR and RGD tracers used in our study.

Indicating increased glucose utilization and the overexpression of pro-angiogenic biomarkers, the investigated tumors displayed steadily increasing radiopharmaceutical uptake from the 1st until the 3rd SRCA transplantation that could be closely connected to increasing metastatic potential and aggressiveness developed during the serial transplantations. This observation reflects some of what has already been reported in the literature. For example, in the mentioned study of Szabó et al. (2022), rising tracer concentrations were registered in the subrenally developing Ne/De tumors and the thoracic metastases during the same experiment. In addition, we hypothesize that the continuous increase in NGR/RGD accumulations may be attributed to enhanced angiogenesis induced by tumor-related hypoxia. Activating pro-angiogenic pathways, hypoxia - derived from the increased oxygen consumption of cancer cells - triggers new blood vessel formation to fulfil the higher oxygen demand during tumor growth and proliferation

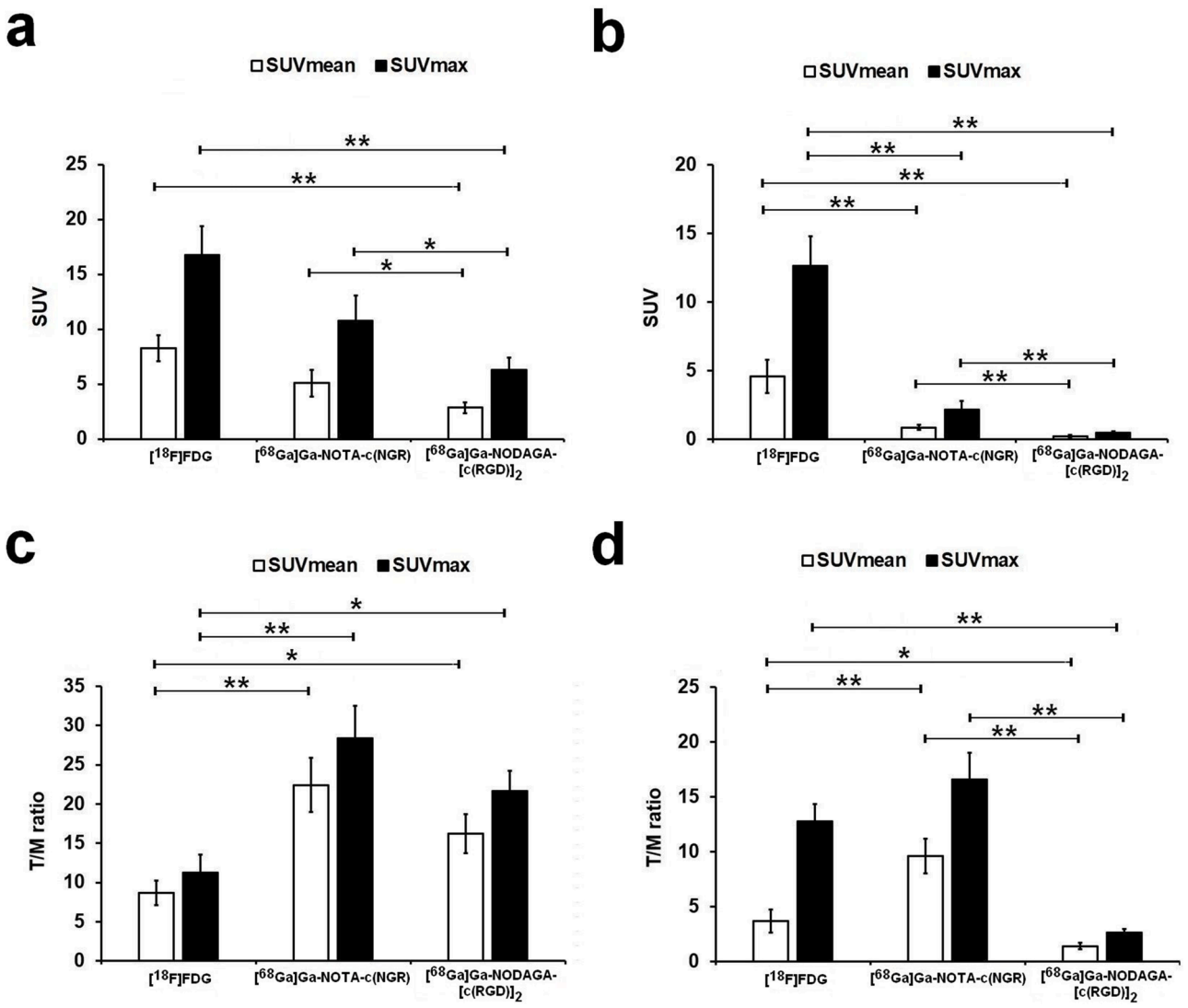

Fig. 6. Quantitative PET data for tertiary He/De tumors (**a** and **c**) and (tertiary) metastatic thoracic parathymic lymph nodes (**b** and **d**) 50 min after [^{18}F]FDG and 90 min after [^{68}Ga]Ga-NOTA-c(NGR)/[^{68}Ga]Ga-NODAGA-[c(RGD)]$_2$ injection. **Panel A** and **B**: SUV mean/max values. **Panel C** and **D**: tumor-to-muscle (T/M) ratios. Statistical significance is marked as $*p \leq 0.05$ and $**p \leq 0.01$. Results are expressed as mean±SD; $n = 3$ rats/tracer. *SD: standard deviation; SUV: standardized uptake value; T/M: tumor-to-muscle ratio.*

Table 2
Quantitative SUV analyses of [^{18}F]FDG, [^{68}Ga]Ga-NOTA-c(NGR) and [^{68}Ga]Ga-NODAGA-[c(RGD)]$_2$ in the metastatic thoracic PTLN derived from the subrenally growing primary (1st transplantation), secondary (2nd transplantation) and tertiary (3rd transplantation) He/De tumors. The uptake values are presented as mean ±SD.

	Metastatic PTLN	[^{18}F]FDG	[^{68}Ga]Ga-NOTA-c(NGR)	[^{68}Ga]Ga-NODAGA-[c(RGD)]$_2$
1st transplantation	SUVmean	2.94±0.87	0.58±0.07	0.09±0.13
	T/M SUVmean	2.52±0.84	6.08±1.13	0.89±0.19
	SUVmax	8.64±1.36	1.24±0.11	0.29±0.40
	T/M SUVmax	7.65±1.38	11.10±1.37	1.25±0.19
2nd transplantation	SUVmean	3.14±0.64	0.69±0.11	0.12±0.06
	T/M SUVmean	2.97±0.87	7.69±1.07	1.17±0.34
	SUVmax	9.07±1.07	1.97±0.60	0.39±0.09
	T/M SUVmax	9.47±1.69	14.58±2.06	1.84±0.24
3rd transplantation	SUVmean	4.59±1.21	0.87±0.17	0.21±0.10
	T/M SUVmean	3.69±1.08	9.61±1.57	1.41±0.31
	SUVmax	12.63±2.17	2.19±0.61	0.49±0.12
	T/M SUVmax	12.74±1.61	16.58±2.47	2.63±0.37

He/De: hepatocellular carcinoma; PTLN: parathymic lymph node; SD: standard deviation; SUV: standardized uptake value; T/M: tumor-to-muscle ratio.

(Koh et al., 2011; Magar et al., 2024; Ziyad, 2011). The abundant expression of angiogenic markers (APN/CD13 and integrin $a_v\beta_3$) on the cells of the newly formed vessels may underlie the enhanced radiotracer uptake that becomes even more prominent during the transplantations as hypoxia and angiogenic activity increase. In our study, however, the elevated tracer accumulation was inferred solely from increasing SUV values observed during transplantations; receptor expression levels were not independently measured.

In addition, despite the methodological similarities between the present study and that of Szabó et al. (2022) the primary Ne/De tumors and their metastases exhibited consistently higher SUV values (2022) than the He/De tumors across all transplantations. For the 1st transplantation the SUVmean of [^{68}Ga]Ga-NOTA-c(NGR) and [^{68}Ga]Ga-NODAGA-RGD/[c(RGD)]$_2$ were 4.12±0.56 (Ne/De) *vs.* 3.69±0.64 (He/De) and 2.05±0.45 (Ne/De) *vs.* 1.34±0.61 (He/De); respectively. In the 2nd transplantation [^{68}Ga]Ga-NOTA-c(NGR) SUVmean was 5.23±0.89 (Ne/De) *vs.* 3.78±0.47 (He/De), and [^{68}Ga]Ga-NODAGA-RGD/[c(RGD)]$_2$ SUVmean was 2.85±0.52 (Ne/De) *vs.* 2.21±0.61 (He/De). During the 3rd transplantation the SUVmean values further increased: [^{68}Ga]Ga-NOTA-c(NGR) 6.35±1.09 (Ne/De) *vs.* 5.09±1.22 (He/De); [^{68}Ga]Ga-NODAGA-RGD/[c(RGD)]$_2$ SUV_{mean}: 3.35±0.63 (Ne/De) *vs.* 2.84±0.51 (He/De). These findings highlight that the tracer accumulation was significantly higher in the Ne/De model throughout the study, despite comparable methodology. According to literature data, the intensity of tumor angiogenesis is highly dependent on the proliferative activity of the individual tumor cells (Ke et al., 2000). Hence, the more enhanced growth rate of the Ne/De tumors and consequential higher angiogenic activity compared to the He/De tumors could be a reasonable explanation for the lower *in vivo* data of the latter neoplasms.

Our PET results demonstrated significantly higher accumulation of [^{68}Ga]Ga-NOTA-c(NGR) than [^{68}Ga]Ga-NODAGA-[c(RGD)]$_2$ in all investigated neoplasms. These *in vivo* observations may reflect a higher expression level of APN/CD13 in the tumors compared to $a_v\beta_3$ integrin. In addition to differences in receptor expression, pharmacokinetic factors such as varying receptor affinity or differences in washout kinetics between the two tracers may also contribute to the registered radiopharmaceutical uptake patterns, however, future verification is needed.

In a like manner, former results on both syngeneic and subrenally growing He/De tumors also indicated similar receptor profiles (Kis et al., 2020; Máté et al., 2015). Although the radiotracer distribution visible at a given investigation time point is mainly reliant on the inherent biological characteristics of the He/De tumors, the observed uptake pattern may be due in part to the pharmacokinetics - particularly the wash-out kinetics - of the radioprobes. Moreover, we registered lower tracer accumulations for the metastatic PTLNs compared to the subrenal lesions. Nevertheless the exact reason behind is not yet full uncovered, we hypothesize some factors that may contribute to the observed phenomenon. Their smaller size, the presence of metabolically inactive necrotic regions within the lymph nodes or the combination of these factors may supply reasonable explanation for the observed tracer uptake.

Overall, the use of radiotracers targeting angiogenesis-related biomolecules overexpressed on tumor cells may allow for a more detailed characterization of tumor biology and associated neovascularization. Precise information on receptor expression patterns of tumors - including receptor density, distribution, and the types of receptors present - appears to be crucial for discovering novel tumor-specific targets that could be used in the *de novo* development of both diagnostic and therapeutic vectors.

5. Limitations

Even though the present study successfully established a rat model of hepatocellular carcinoma that enables the detailed assessment of metastatic spread *in vivo*, this model has certain limitations that warrant further consideration. Unlike conventional syngeneic hepatocellular carcinoma models, which typically involve orthotopic implantation into hepatic tissue (Macek et al., 2019), the tumor cells in this study were transplanted under the left renal capsule. Due to the ectopic implantation site, the model lacks the characteristic fibrotic or cirrhotic liver microenvironment associated with hepatocellular carcinoma. Consequently, it does not fully recapitulate the complex tumor microenvironment, including stromal and vascular components, thereby limiting its utility for comprehensive investigations of tumor-immune interplay in hepatocellular carcinoma.

6. Conclusion

This study demonstrates that radiolabelled NGR and RGD probes can detect angiogenesis *in vivo* in slow-growing hepatocellular carcinoma models. Continuous increase in tumor tracer uptake during the serial transplantations might not only represent the *in vivo* behaviour of each lesion but also the temporal changes in angiogenic biomarker expression upon tumor progression. A better understanding of tumor receptor profiles could support the development of novel diagnostic tools and targeted therapeutic approaches, including theranostics or targeted radiotherapy, thereby offering opportunities for more personalized and effective cancer management strategies.

Funding

Funding was received from the KDP-2021 program of the Ministry for Innovation and Technology from the source of the national research, development and innovation fund (Gy.T. and I. K-SZ.).

Ethics approval

Principles of the Ethics Committee for Animal Experimentation of the United Kingdom were followed, and the local Ethics Committee for Animal Experimentation approved the experiment (University of Debrecen, approval number: 28/2023/DEMÁB).

CRediT authorship contribution statement

Alexandra Barkóczi: Writing – original draft, Visualization, Methodology, Investigation, Data curation. **Zita Képes:** Writing – review & editing, Writing – original draft, Visualization, Validation, Conceptualization. **Judit P. Szabó:** Methodology, Investigation. **Renáta Adél Dienes:** Methodology, Investigation. **Péter Kálmán Károlyi:** Methodology, Investigation. **Tamás Papp:** Visualization, Methodology, Investigation. **Ibolya Kálmán-Szabó:** Methodology, Investigation. **Tamás Sass:** Investigation. **Gábor Opposits:** Validation, Methodology, Investigation, Data curation. **István Kertész:** Validation, Methodology, Investigation. **István Hajdu:** Validation, Methodology, Investigation, Data curation. **György Trencsényi:** Writing – review & editing, Writing – original draft, Visualization, Conceptualization. **Ádám Deák:** Writing – review & editing, Writing – original draft, Conceptualization.

Declaration of competing interest

The authors have declared that no competing interest exists.

Data Availability

The datasets used and/or analysed during the current study are available from the corresponding author upon reasonable request.

References

Akhavan, O., Ghaderi, E., 2013. Graphene nanomesh promises extremely efficient *in vivo* photothermal therapy. Small 9, 3593–3601. https://doi.org/10.1002/smll.201203106.

Ando, K., Hu, Q., Kasagi, Y., Oki, E., Mori, M., 2021. Recent developments in cancer research: expectations for a new remedy. Ann. Gastroenterol. Surg. 5, 419–426. https://doi.org/10.1002/ags3.12440.

Arató, V., Képes, Z., Szabó, J.P., Farkasinszky, G., Sass, T., Dénes, N., Kis, A., Opposits, G., Jószai, I., Kálmán, F.K., Hajdu, I., Trencsényi, G., Kertész, I., 2024. Acute myelomonoblastic leukemia (My1/De): a preclinical rat model. In Vivo. 38, 1064–1073. https://doi.org/10.21873/invivo.13540.

Assali, A., Akhavan, O., Adeli, M., Razzazan, S., Dinarvand, R., Zanganeh, S., Soleimani, M., Dinarvand, M., Atyabi, F., 2018. Multifunctional core-shell nanoplatforms (gold@graphene oxide) with mediated NIR thermal therapy to promote miRNA delivery. Nanomedicine 14, 1891–1903. https://doi.org/10.1016/j.nano.2018.05.016.

Bieker, R., Kessler, T., Schwöppe, C., Padró, T., Persigehl, T., Bremer, C., Dreischalück, J., Kolkmeyer, A., Heindel, W., Mesters, R.M., Berdel, W.E., 2009. Infarction of tumor vessels by NGR-peptide-directed targeting of tissue factor: experimental results and first-in-man experience. Blood 113, 5019–5027. https://doi.org/10.1182/blood-2008-04-150318.

Biemar, F., Foti, M., 2013. Global progress against cancer-challenges and opportunities. Cancer. Biol. Med. 10, 183–186. https://doi.org/10.7497/j.issn.2095-3941.2013.04.001.

Bryda, E.C., 2013. The Mighty Mouse: the impact of rodents on advances in biomedical research. Mo. Med. 110, 207–211.

Cai, W., Chen, X., 2006. Anti-angiogenic cancer therapy based on integrin alphavbeta3 antagonism. Anticancer. Agents. Med. Chem. 6, 407–428. https://doi.org/10.2174/187152006778226530.

Chen, K., Ma, W., Li, G., Wang, J., Yang, W., Yap, L.P., Hughes, L.D., Park, R., Conti, P.S., 2013. Synthesis and evaluation of 64Cu-labeled monomeric and dimeric NGR peptides for MicroPET imaging of CD13 receptor expression. Mol. Pharm. 10, 417–427. https://doi.org/10.1021/mp3005676.

Cunha, L., Horvath, I., Ferreira, S., Lemos, J., Costa, P., Vieira, D., Veres, D.S., Szigeti, K., Summavielle, T., Máthé, D., Metello, L.F., 2014. Preclinical imaging: an essential ally in modern biosciences. Mol. Diagn. Ther. 18, 153–173. https://doi.org/10.1007/s40291-013-0062-3.

Cyagen Knockout Catalog Models, 2020. Newsletter, research trend. https://www.cyagen.com/us/en/community/technical-bulletin/rat-model.html (accessed 16 November 2024).

Dezso, B., Rady, P., Morocz, I., Varga, E., Gomba, S., Poulsen, K., Kertai, P., 1990. Morphological and immunohistochemical characteristics of dimethylnitrosamine-induced malignant mesenchymal renal tumor in F-344 rats. J. Cancer. Res. Clin. Oncol. 116, 372–378. https://doi.org/10.1007/BF01612920.

Eur. Comm, 2019. 2019 Report On the Statistics On the Use of Animals For Scientific Purposes in the Member States of the European Union in 2015-2017, 2019. Rep. Eur. Comm., Brussels.

Faintuch, B.L., Oliveira, E.A., Targino, R.C., Moro, A.M., 2014. Radiolabeled NGR phage display peptide sequence for tumor targeting. Appl. Radiat. Isot. 86, 41–45. https://doi.org/10.1016/j.apradiso.2013.12.035.

Fazaeli, Y., Akhavan, O., Rahighi, R., Aboudzadeh, M.R., Karimi, E., Afarideh, H., 2014. *In vivo* SPECT imaging of tumors by 198,199Au-labeled graphene oxide nanostructures. Mater. Sci. Eng. C. Mater. Biol. Appl. 45, 196–204. https://doi.org/10.1016/j.msec.2014.09.019.

Fidler, I.J., 1970. Metastasis: quantitative analysis of distribution and fate of tumor emboli labeled with ^{125}I-5-iodo-2′-deoxyuridine. J. Natl. Cancer. Inst. 45, 773–782.

Florea, A., Mottaghy, F.M., Bauwens, M., 2021. Molecular imaging of angiogenesis in oncology: current preclinical and clinical status. Int. J. Mol. Sci. 22, 5544. https://doi.org/10.3390/ijms22115544.

Gao, Y., Wang, Z., Ma, X., Ma, W., Zhao, M., Fu, T., Li, G., Wang, S., Wang, Z., Yang, W., Kang, F., Wang, J., 2017. The uptake exploration of 68Ga-labeled NGR in well-differentiated hepatocellular carcinoma xenografts: indication for the new clinical translational of a tracer based on NGR. Oncol. Rep. 38, 2859–2866. https://doi.org/10.3892/or.2017.5933.

Giacobbe, A., Abate-Shen, C., 2021. Modeling metastasis in mice: a closer look. Trends. Cancer. 7, 916–929. https://doi.org/10.1016/j.trecan.2021.06.010.

Glenny, E.M., Coleman, M.F., Giles, E.D., Wellberg, E.A., Hursting, S.D., 2021. Designing relevant preclinical rodent models for studying links between nutrition, obesity, metabolism, and cancer. Annu. Rev. Nutr. 41, 253–282. https://doi.org/10.1146/annurev-nutr-120420-032437.

Guan, X., 2015. Cancer metastases: challenges and opportunities. Acta. Pharm. Sin. B. 5, 402–418. https://doi.org/10.1016/j.apsb.2015.07.005.

Guo, J., Higashi, K., Ueda, Y., Oguchi, M., Takegami, T., Toga, H., Sakuma, T., Yokota, H., Katsuda, S., Tonami, H., Yamamoto, I., 2006. Microvessel density: correlation with 18F-FDG uptake and prognostic impact in lung adenocarcinomas. J. Nucl. Med. 47, 419–425.

Hart, I.R., Fidler, I.J., 1980. Role of organ selectivity in the determination of metastatic patterns of B16 melanoma. Cancer. Res. 40, 2281–2287.

Hebert, J.D., Neal, J.W., Winslow, M.M., 2023. Dissecting metastasis using preclinical models and methods. Nat. Rev. Cancer. 23, 391–407. https://doi.org/10.1038/s41568-023-00568-4.

Jiang, L., Tu, Y., Shi, H., Cheng, Z., 2014. PET probes beyond (18)F-FDG. J. Biomed. Res. 28, 435–446. https://doi.org/10.7555/JBR.28.20130196.

Kang, Y., Siegel, P.M., Shu, W., Drobnjak, M., Kakonen, S.M., Cordón-Cardo, C., Guise, T. A., Massagué, J., 2003. A multigenic program mediating breast cancer metastasis to bone. Cancer. Cell. 3, 537–549. https://doi.org/10.1016/s1535-6108(03)00132-6.

Kawamura, J., Shimada, Y., Kitaichi, H., Komoto, I., Hashimoto, Y., Kaganoi, J., Miyake, M., Yamasaki, S., Kondo, K., Imamura, M., 2007. Clinicopathological significance of aminopeptidase N/CD13 expression in human gastric carcinoma. Hepatogastroenterology 54, 36–40.

Ke, L.D., Shi, Y.X., Im, S.A., Chen, X., Yung, W.K., 2000. The relevance of cell proliferation, vascular endothelial growth factor, and basic fibroblast growth factor production to angiogenesis and tumorigenicity in human glioma cell lines. Clin. Cancer. Res. 6, 2562–2572.

Kis, A., Szabó, J.P., Dénes, N., Vágner, A., Nagy, G., Garai, I., Fekete, A., Szikra, D., Hajdu, I., Matolay, O., Méhes, G., Mező, G., Kertész, I., Trencsényi, G., 2020. *In vivo* imaging of hypoxia and neoangiogenesis in experimental syngeneic hepatocellular carcinoma tumor model using positron emission tomography. Biomed. Res. Int. 2020, 4952372. https://doi.org/10.1155/2020/4952372.

Koh, M.Y., Lemos, R., Liu, X., Powis, G., 2011. The hypoxia associated factor switches cells from HIF-1α- to HIF-2α-dependent signaling promoting stem cell characteristics, aggressive tumor growth and invasion. Cancer. Res. 71, 4015–4027. https://doi.org/10.1158/0008-5472.CAN-10-4142.

Kuczynski, E.A., Yin, M., Bar-Zion, A., Lee, C.R., Butz, H., Man, S., Daley, F., Vermeulen, P.B., Yousef, G.M., Foster, F.S., Reynolds, A.R., Kerbel, R.S., 2016. Co-option of liver vessels and not sprouting angiogenesis drives acquired sorafenib resistance in hepatocellular carcinoma. J. Natl. Cancer. Inst. 108, djw030. https://doi.org/10.1093/jnci/djw030.

Kwitek-Black, A.E., Jacob, H.J., 2001. The use of designer rats in the genetic dissection of hypertension. Curr. Hypertens. Rep. 3, 12–18. https://doi.org/10.1007/s11906-001-0072-0.

Li, G., Wang, X., Zong, S., Wang, J., Conti, P.S., Chen, K., 2014. MicroPET imaging of CD13 expression using a (64)Cu-labeled dimeric NGR peptide based on sarcophagine cage. Mol. Pharm. 11, 3938–3946. https://doi.org/10.1021/mp500354x.

Li, D., Zhang, J., Ji, N., Zhao, X., Zheng, K., Qiao, Z., Li, F., Lang, L., Iagaru, A., Niu, G., Zhu, Z., Chen, X., 2018. Combined 68Ga-NOTA-PRGD2 and 18F-FDG PET/CT can discriminate uncommon meningioma mimicking high-grade glioma. Clin. Nucl. Med. 43, 648–654. https://doi.org/10.1097/RLU.0000000000002233.

Lien, V.T., Celen, S., Nuruddin, S., Attili, B., Doumont, G., Van Simaeys, G., Bormans, G., Klaveness, J., Olberg, D.E., 2021. Preclinical evaluation of [^{18}F]cabozantinib as a PET imaging agent in a prostate cancer mouse model. Nucl. Med. Biol. 93, 74–80. https://doi.org/10.1016/j.nucmedbio.2020.12.002.

Liu, Z., Dong, S., Liu, M., Liu, Y., Ye, Z., Zeng, J., Yao, M., 2023. Experimental models for cancer brain metastasis. Cancer. Pathog. Ther. 2, 15–23. https://doi.org/10.1016/j.cpt.2023.10.005.

Máté, G., Kertész, I., Enyedi, K.N., Mező, G., Angyal, J., Vasas, N., Kis, A., Szabó, É., Emri, M., Bíró, T., Galuska, L., Trencsényi, G., 2015. *In vivo* imaging of aminopeptidase N (CD13) receptors in experimental renal tumors using the novel radiotracer (68)Ga-NOTA-c(NGR). Eur. J. Pharm. Sci. 69, 61–71. https://doi.org/10.1016/j.ejps.2015.01.002.

Ma, W., Kang, F., Wang, Z., Yang, W., Li, G., Ma, X., Li, G., Chen, K., Zhang, Y., Wang, J., 2013. (99m)Tc-labeled monomeric and dimeric NGR peptides for SPECT imaging of CD13 receptor in tumor-bearing mice. Amino. Acids. 44, 1337–1345. https://doi.org/10.1007/s00726-013-1469-1.

Ma, W., Shao, Y., Yang, W., Li, G., Zhang, Y., Zhang, M., Zuo, C., Chen, K., Wang, J., 2016. Evaluation of (188)re-labeled NGR-VEGI protein for radioimaging and radiotherapy in mice bearing human fibrosarcoma HT-1080 xenografts. Tumour. Biol. 37, 9121–9129. https://doi.org/10.1007/s13277-016-4810-y.

Macek Jilkova, Z., Kurma, K., Decaens, T., 2019. Animal models of hepatocellular carcinoma: the role of immune system and tumor microenvironment. Cancers (Basel) 11, 1487. https://doi.org/10.1016/10.3390/cancers11101487.

Magar, A.G., Morya, V.K., Kwak, M.K., Oh, J.U., Noh, K.C., 2024. A molecular perspective on HIF-1α and angiogenic stimulator networks and their role in solid tumors: an update. Int. J. Mol. Sci. 25, 3313. https://doi.org/10.3390/ijms25063313.

Minn, A.J., Gupta, G.P., Siegel, P.M., Bos, P.D., Shu, W., Giri, D.D., Viale, A., Olshen, A. B., Gerald, W.L., Massagué, J., 2005. Genes that mediate breast cancer metastasis to lung. Nature 436, 518–524. https://doi.org/10.1038/nature03799.

Miranda, A., Bertoglio, D., Stroobants, S., Staelens, S., Verhaeghe, J., 2021. Translation of preclinical PET imaging findings: challenges and motion correction to overcome the confounding effect of anesthetics. Front. Med. (Lausanne). 8, 753977. https://doi.org/10.3389/fmed.2021.753977.

Mukherjee, P., Roy, S., Ghosh, D., Nandi, S.K., 2022. Role of animal models in biomedical research: a review. Lab. Anim. Res. 38, 18. https://doi.org/10.1186/s42826-022-00128-1.

Murakami, H., Yokoyama, A., Kondo, K., Nakanishi, S., Kohno, N., Miyake, M., 2005. Circulating aminopeptidase N/CD13 is an independent prognostic factor in patients with non-small cell lung cancer. Clin. Cancer. Res. 11, 8674–8679. https://doi.org/10.1158/1078-0432.CCR-05-1005.

Nolan, D.J., Ciarrocchi, A., Mellick, A.S., Jaggi, J.S., Bambino, K., Gupta, S., Heikamp, E., McDevitt, M.R., Scheinberg, D.A., Benezra, R., Mittal, V., 2007. Bone marrow-derived endothelial progenitor cells are a major determinant of nascent tumor neovascularization. Genes. Dev. 21, 1546–1558. https://doi.org/10.1101/gad.436307.

Parker, A.L., Benguigui, M., Fornetti, J., Goddard, E., Lucotti, S., Insua-Rodríguez, J., Wiegmans, A.P., Early Career Leadership Council of the Metastasis Research Society, 2022. Current challenges in metastasis research and future innovation for clinical translation. Clin. Exp. Metastasis. 39, 263–277. https://doi.org/10.1007/s10585-021-10144-5.

Pasqualini, R., Koivunen, E., Kain, R., Lahdenranta, J., Sakamoto, M., Stryhn, A., Ashmun, R.A., Shapiro, L.H., Arap, W., Ruoslahti, E., 2000. Aminopeptidase N is a receptor for tumor-homing peptides and a target for inhibiting angiogenesis. Cancer. Res. 60, 722–727.

Phelps, M.E., 2000a. PET: the merging of biology and imaging into molecular imaging. J. Nucl. Med. 41, 661–681.

Phelps, M.E., 2000b. Positron emission tomography provides molecular imaging of biological processes. Proc. Nat. Acad. Sci. USA. 97, 9226–9233. https://doi.org/10.1073/pnas.97.16.9226.

Rozsa, D., Trencsenyi, G., Kertai, P., Marian, T., Nagy, G., Banfalvi, G., 2009. Lymphatic spread of mesenchymal renal tumor to metastatic parathymic lymph nodes in rat. Histol. Histopathol. 24, 1367–1379. https://doi.org/10.14670/HH-24.1367.

Sajjad, H., Imtiaz, S., Noor, T., Siddiqui, Y.H., Sajjad, A., Zia, M., 2021. Cancer models in preclinical research: a chronicle review of advancement in effective cancer research. Animal. Model. Exp. Med. 4, 87–103. https://doi.org/10.1002/ame2.12165.

Seyfried, T.N., Huysentruyt, L.C., 2013. On the origin of cancer metastasis. Crit. Rev. Oncog. 18, 43–73. https://doi.org/10.1615/critrevoncog.v18.i1-2.40.

Shao, Y., Liang, W., Kang, F., Yang, W., Ma, X., Li, G., Zong, S., Chen, K., Wang, J., 2014a. A direct comparison of tumor angiogenesis with ^{68}ga-labeled NGR and RGD peptides in HT-1080 tumor xenografts using microPET imaging. Amino. Acids. 46, 2355–2364. https://doi.org/10.1007/s00726-014-1788-x.

Shao, Y., Liang, W., Kang, F., Yang, W., Ma, X., Li, G., Zong, S., Chen, K., Wang, J., 2014b. 68Ga-labeled cyclic NGR peptide for microPET imaging of CD13 receptor expression. Molecules 19, 11600–11612. https://doi.org/10.3390/molecules190811600.

Sharma, G., Goyal, Y., Bhatia, S., 2023. Preclinical animal models of cancer: applications and limitations. In: Pathak, S., Banerjee, A., Bisgin, A. (Eds.), Handbook of Animal Models and Its Uses in Cancer Research. Springer., Singapore, pp. 1051–1071.

Soudy, R., Ahmed, S., Kaur, K., 2012. NGR peptide ligands for targeting CD13/APN identified through peptide array screening resemble fibronectin sequences. ACS. Comb. Sci. 14, 590–599. https://doi.org/10.1021/co300055s.

Szabo, J.P., Denes, N., Arato, V., Racz, S., Kis, A., Opposits, G., Kepes, Z., Hajdu, I., Joszai, I., Emri, M., Kertesz, I., Mezo, G., Trencsenyi, G., 2022. *In vivo* imaging of neo-angiogenesis of transplanted metastases in subrenal capsule assay induced rat model. *In Vivo* (Brooklyn) 36, 1667–1675. https://doi.org/10.21873/invivo.12878.

Toriihara, A., Duan, H., Thompson, H.M., Park, S., Hatami, N., Baratto, L., Fan, A.C., Iagaru, A., 2019. ^{18}F-FPPRGD$_2$ PET/CT in patients with metastatic renal cell cancer. Eur. J. Nucl. Med. Mol. Imaging 46, 1518–1523. https://doi.org/10.1007/s00259-019-04295-7.

Trencsényi, G., Halmos, G., Képes, Z., 2023. Radiolabeled NGR-based heterodimers for angiogenesis imaging: a review of preclinical studies. Cancers (Basel) 15, 4459. https://doi.org/10.3390/cancers15184459.

Trencsenyi, G., Kertai, P., Bako, F., Hunyadi, J., Marian, T., Hargitai, Z., Pocsi, I., Muranyi, E., Hornyak, L., Banfalvi, G., 2009. Renal capsule-parathymic lymph node complex: a new *in vivo* metastatic model in rats. Anticancer. Res. 29, 2121–2126.

Trencsenyi, G., Nagy, G., Kahlik, B., Nemeth, E., Kertai, P., Kiss, A., Banfalvi, G., 2014a. Lymphoid metastasis of rat My2/De leukemia. Leuk. Res. 38, 586–593. https://doi.org/10.1016/j.leukres.2014.02.006.

Trencsenyi, G., Marian, T., Bako, F., Emri, M., Nagy, G., Kertai, P., Banfalvi, G., 2014b. Metastatic hepatocarcinoma He/de tumor model in rat. J. Cancer. 5, 548–558. https://doi.org/10.7150/jca.9315.

Vatsa, R., Ashwathanarayana, A.G., Singh, G., Kavanal, A.J., Kumar, S., Rana, N., Shukla, J., Mittal, B.R., 2019. A comparison of angiogenesis and glycolytic imaging in patients with clinical suspected locally advanced breast cancer. Clin. Nucl. Med. 44, e479–e483. https://doi.org/10.1097/RLU.0000000000002647.

Wakefield, L., Agarwal, S., Tanner, K., 2023. Preclinical models for drug discovery for metastatic disease. Cell 186, 1792–1813. https://doi.org/10.1016/j.cell.2023.02.026.

Wang, F., Sun, Q., Feng, B., Xu, Z., Zhang, J., Xu, J., Lu, L., Yu, H., Wang, M., Li, Y., Zhang, W., 2016. Polydopamine-functionalized graphene oxide loaded with gold nanostars and doxorubicin for combined photothermal and chemotherapy of metastatic breast cancer. Adv. Healthc. Mater. 5, 2227–2236. https://doi.org/10.1002/adhm.201600283.

Weis, S.M., Cheresh, D.A., 2011. αV integrins in angiogenesis and cancer. Cold. Spring. Harb. Perspect. Med. 1, a006478. https://doi.org/10.1101/cshperspect.a006478.

Wong, P.P., Demircioglu, F., Ghazaly, E., Alrawashdeh, W., Stratford, M.R., Scudamore, C.L., Cereser, B., Crnogorac-Jurcevic, T., McDonald, S., Elia, G., Hagemann, T., Kocher, H.M., Hodivala-Dilke, K.M., 2015. Dual-action combination therapy enhances angiogenesis while reducing tumor growth and spread. Cancer. Cell. 27, 123–137. https://doi.org/10.1016/j.ccell.2014.10.015.

Zhang, J., Lu, X., Wan, N., Hua, Z., Wang, Z., Huang, H., Yang, M., Wang, F., 2014. 68Ga-DOTA-NGR as a novel molecular probe for APN-positive tumor imaging using MicroPET. Nucl. Med. Biol. 41, 268–275. https://doi.org/10.1016/j.nucmedbio.2013.12.008.

Zheng, S., Chen, Z., Huang, C., Chen, Y., Miao, W., 2019. [^{99m}Tc]3PRGD$_2$ for integrin receptor imaging of esophageal cancer: a comparative study with [^{18}F]FDG PET/CT. Ann. Nucl. Med. 33, 135–143. https://doi.org/10.1007/s12149-018-1315-3.

Zhu, A., Lee, D., Shim, H., 2011. Metabolic positron emission tomography imaging in cancer detection and therapy response. Semin. Oncol. 38, 55–69. https://doi.org/10.1053/j.seminoncol.2010.11.012.

Zhu, L., Ding, Z., Li, X., Wei, H., Chen, Y., 2020. Research progress of radiolabeled asn-gly-arg (NGR) peptides for imaging and therapy. Mol. Imaging. 19, 1536012120934957. https://doi.org/10.1177/1536012120934957.

Ziyad, S., Iruela-Arispe, M.L., 2011. Molecular mechanisms of tumor angiogenesis. Genes. Cancer. 2, 1085–1096. https://doi.org/10.1177/1947601911432334.

Zucali, P.A., Simonelli, M., De Vincenzo, F., Lorenzi, E., Perrino, M., Bertossi, M., Finotto, R., Naimo, S., Balzarini, L., Bonifacio, C., Timofeeva, I., Rossoni, G., Mazzola, G., Lambiase, A., Bordignon, C., Santoro, A., 2013. Phase I and pharmacodynamic study of high-dose NGR-hTNF in patients with refractory solid tumours. Br. J. Cancer. 108, 58–63. https://doi.org/10.1038/bjc.2012.506.